

Modeling and Optimization of High-Power Nd³⁺-Yb³⁺ Codoped Fiber Lasers

Eldad Yahel, Ortwin Hess, and Amos A. Hardy, *Fellow, IEEE, Fellow, OSA*

Abstract—High-power continuous-wave Nd³⁺-Yb³⁺ codoped fiber lasers (NYDFL) are analyzed, based on a rate-propagation equations model. The model takes into account energy transfer between Nd³⁺ and Yb³⁺, as well as cross relaxation between Nd³⁺ ions, and contributions from high-order modes to the amplified spontaneous emission (ASE). Examples of cladding-pumped NYDFLs with distributed Bragg reflector (DBR) at either end are presented. We demonstrate the optimal laser design by considering the effects of the Nd³⁺ and Yb³⁺ concentrations, pump wavelengths multiplexing, output mirror reflectivity, and the laser wavelength. Approximate quasi-analytical solutions are shown to be in good agreement with the exact numerical solutions of the rate equations for practical conditions.

Index Terms—Distributed Bragg reflector (DBR) lasers, Neodymium (Nd), optical fiber lasers, optical fiber theory, Ytterbium (Yb).

I. INTRODUCTION

RARE-EARTH-DOPED fiber lasers demonstrate an excellent combination of high efficiency and high spatial beam quality, which makes them attractive compared to conventional solid-state lasers. For high-power fiber laser applications (e.g., printing, free-space communication), Ytterbium-doping results in a very efficient lasing transition with broad emission and absorption bands, allowing various pumping schemes and a wide tuning range of the laser wavelength. Furthermore, the simple two-level energy manifold structure of the Yb³⁺ ion makes it relatively free of concentration quenching, allowing shorter fiber lasers with reduced nonlinearities. These excellent features have led to the realization of high-power cladding-pumped Yb³⁺-doped fiber lasers (YDFL) [1]–[3].

It is possible to increase further the output power, and extend the pumping schemes of YDFLs by using several wavelength multiplexed diode lasers as the pump source. To this end, Nd³⁺-Yb³⁺ glass is doped with both the Nd³⁺ and Yb³⁺ ions, which allows pumping the Yb³⁺ ions indirectly through a nonradiative energy transfer from the Nd³⁺ ions [4], [5]. Furthermore, both Nd³⁺ and Yb³⁺ emit in the wavelength range of $\sim 1 \mu\text{m}$, and thus the output power from cladding-pumped Nd³⁺-Yb³⁺ codoped fiber lasers (NYDFL) can be

Manuscript received April 27, 2005; revised October 18, 2005. The work of A. Hardy was supported by the Chana and Heinrich Manderman Chair in Optoelectronics.

E. Yahel and O. Hess are with the Advanced Technology Institute, University of Surrey Guildford, Surrey GU2 7XH, U.K. (e-mail: E.Yahel@surrey.ac.uk; O.Hess@surrey.ac.uk)

A. A. Hardy is with the Department of Electrical Engineering–Physical Electronics, Tel Aviv University, Tel Aviv 69978, Israel (e-mail: hardy@eng.tau.ac.il).

Digital Object Identifier 10.1109/JLT.2005.863324

scaled to hundreds of watts [6], [7]. In order to achieve such high output powers without reaching the threshold of nonlinear effects, the dimensions of the fiber core must be increased and the fiber becomes intrinsically multimode [8]. Bending losses can be applied to discriminate the fundamental LP₀₁ mode from higher order modes so that the laser output becomes practically single mode [9].

Previous works that model high-power rare-earth-doped fiber lasers have been limited to single-ion systems, such as Nd³⁺ or Yb³⁺ [10] or other codoped systems, e.g., Er³⁺-Yb³⁺ [11]. Our goal here is to extend these works and to demonstrate models of NYDFLs based on numerical calculations of detailed coupled rate-propagation equations. Our model takes into account the energy transfer between Nd³⁺ and Yb³⁺ ions, cross relaxation among Nd³⁺ ions, Nd³⁺ clustering effects, spectrally resolved amplified spontaneous emission (ASE) of Nd³⁺ and Yb³⁺ ions, and scattering losses. Our model also accounts approximately for contribution of high-order modes to the ASE. We also present a quasi-analytical model to approximate the exact equations. Nonlinear effects (e.g., stimulated Brillouin scattering, self-phase modulation), however, are disregarded in the present calculations.

The structure of this contribution is the following. In Section II, we describe the set of coupled rate-propagation equations for the Nd³⁺-Yb³⁺ system. The approximate quasi-analytical solutions are described in Section III. In Section IV, we consider some numerical examples for cladding-pumped high-power NYDFLs. In particular, we discuss the effects of several key design parameters (e.g., the pump power, fiber length, pump configuration, pump wavelengths, output mirror reflectivity, laser wavelength, and the Nd³⁺ and Yb³⁺ concentrations) on the laser output power and efficiency. We also demonstrate the effect of Nd³⁺ clustering on the laser performance, and compare the approximate solutions of the quasi-analytical model to the exact numerical solutions. Finally, conclusions are given in Section V. The main derivation steps of the approximate solution are described in the Appendix.

II. THEORETICAL MODEL

We assume a double-clad fiber laser of length L with distributed Bragg reflector (DBR) mirrors at either side. The wavelength-dependent power reflectivities of the DBR mirrors are $R_1(\lambda)$ and $R_2(\lambda)$ at $z = 0$ and $z = L$, respectively. The pump power $P_p^\pm(z, t)$ at the wavelength λ_p is injected into the first cladding either at $z = 0$ or at $z = L$, where the positive or negative superscripts denote propagation in the forward or backward z -direction, respectively. It is assumed that due to

fiber bending and special double-clad fiber geometries, the pump-power absorption along the fiber length is essentially uniform, and it can be associated with an effective power filling factor Γ_p . The value of Γ_p can be higher than the ratio of the core area (A_{core}) to the combined area of the core and the first cladding (A_{clad}), due to the increased pump absorption in a bent fiber [12], [13]. The spectral power density of the light that propagates in the laser cavity is denoted $P^\pm(z, t, \lambda)$, with a wavelength-dependent power filling factor $\Gamma(\lambda)$. We assume that $\Gamma(\lambda)$ is given by the ratio of the multimode power that is guided and amplified in the core to the total power propagating in the fiber. We also assume that unguided radiation modes can be neglected, and that the contribution to the amplified power in the core from interference of guided modes is insignificantly small for practical values of the fiber V-number [14]. Under these assumptions, an approximate expression for the power filling factor $\Gamma(\lambda)$ can be derived based on [15], namely

$$\Gamma(\lambda) \simeq \frac{\sum_{\eta} |u_{\eta}(\lambda)|^2 \Gamma_{\eta}(\lambda) I_{\eta} g_{\eta}}{\sum_{\eta} |u_{\eta}(\lambda)|^2 I_{\eta} g_{\eta}}. \quad (1)$$

Here, $\Gamma_{\eta}(\lambda)$ is the modal power filling factor, $u_{\eta}(\lambda)$ is the modal coefficient in the expansion of the total field in terms of the guided transverse modes, and η is the modal index (i.e., $\eta = 1$ corresponds to the fundamental LP_{01} mode). Thus, $|u_{\eta}(\lambda)|^2$ is proportional to the power carried by the mode η , and can in principle also depend on the spatial coordinate z (due to, e.g., mode coupling). Other parameters in (1) are the modal degeneracy value g_{η} [16] and the modal normalization I_{η} that is proportional to an integral of the modal envelope over an infinite cross section [15]. An approximate expression for $\Gamma_{\eta}(\lambda)$ of the fundamental and higher order LP modes is given in [15]. In what follows, we assume that due to specialized fiber coiling techniques most of the higher order modes are practically suppressed [7]. It is therefore sufficient to include only the first two guided modes in (1), i.e., the LP_{01} and LP_{11} modes.

We assume that the Nd^{3+} and Yb^{3+} ions are uniformly doped over the core cross section with concentrations N_{Nd} and N_{Yb} , respectively. Our model includes forward and backward energy transfer between Nd^{3+} and Yb^{3+} ions, cross relaxation of Nd^{3+} ions, and Nd^{3+} and Yb^{3+} single-ion transitions (cf. Fig. 1). We note that unlike the Er^{3+} - Yb^{3+} codoped system, where the main energy-transfer channel is from the Yb^{3+} ions to the Er^{3+} acceptors [17], here, the Yb^{3+} ions are the energy acceptors from the Nd^{3+} donors. It is assumed that the Yb^{3+} ions are coupled with Nd^{3+} ions through a dipole-dipole type interaction process [4]. However, some of the Nd^{3+} ions can form clusters, in particular in high Nd^{3+} concentration fibers [18], [19], and these clustered Nd^{3+} are not coupled to the Yb^{3+} ions. In a Nd^{3+} cluster, the cross-relaxation interaction of the Nd^{3+} ions is accelerated since the average distance between Nd^{3+} ions is relatively short [19]. We also assume that the populations of the manifolds ${}^4I_{15/2}$, ${}^4I_{13/2}$, and ${}^4I_{11/2}$ are virtually empty, due to the fast nonradiative transition times of these levels. Therefore, we impose $N_3 = N_2 = N_1 \simeq 0$ (and equivalently $\bar{N}_3 = \bar{N}_2 = \bar{N}_1 \simeq 0$ for the clustered populations; cf. Fig. 1). The pump photons are absorbed by the Nd^{3+}

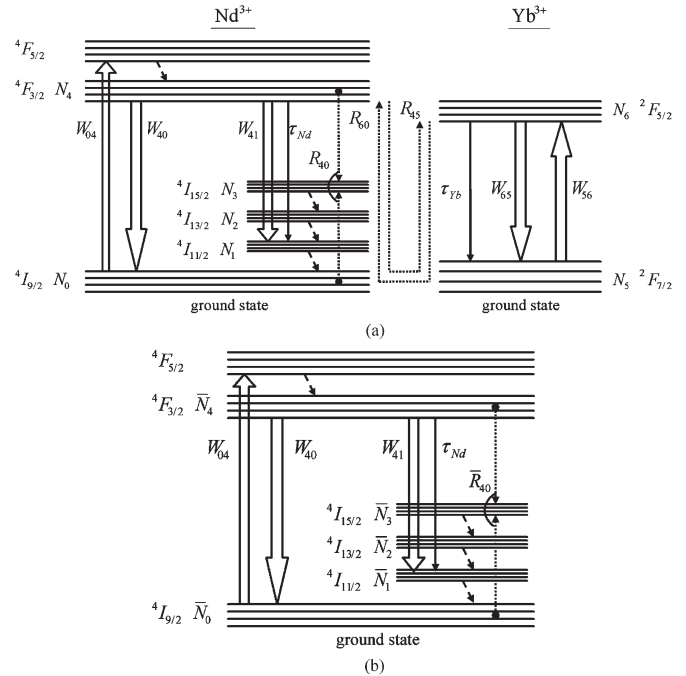


Fig. 1. Energy-level diagram for the Nd^{3+} - Yb^{3+} codoped system. (a) Homogeneous Nd^{3+} - Yb^{3+} system. (b) Clustered Nd^{3+} system.

ions in the ground manifold ${}^4I_{9/2}$, exciting them to the manifold ${}^4F_{5/2}$, from where they instantly decay to the manifold ${}^4F_{3/2}$. Pump photons are also absorbed by the Yb^{3+} ions in the ground manifold ${}^2F_{7/2}$, exciting them to the manifold ${}^2F_{5/2}$. Losses to the ${}^4F_{3/2}$ state by excited state absorption (ESA) of pump photons or by upconversion to higher level manifolds are neglected due to the small population of this manifold. With these assumptions, the populations of the homogeneous and the clustered ions satisfy the following rate equations:

$$\begin{aligned} \frac{\partial}{\partial t} N_4(z, t) &= -N_4(z, t) \left[\frac{1}{\tau_{\text{Nd}}} + W_{04}(z, t) + W_{40}(z, t) + W_{41}(z, t) \right] \\ &\quad + W_{04}(z, t)(1 - k)N_{\text{Nd}} - R_{45}N_4(z, t)[N_{\text{Yb}} - N_6(z, t)] \\ &\quad + R_{60}N_6(z, t)[(1 - k)N_{\text{Nd}} - N_4(z, t)] \\ &\quad - R_{40}N_4(z, t)[(1 - k)N_{\text{Nd}} - N_4(z, t)] \end{aligned} \quad (2)$$

$$\begin{aligned} \frac{\partial}{\partial t} N_6(z, t) &= -N_6(z, t) \left[\frac{1}{\tau_{\text{Yb}}} + W_{56}(z, t) + W_{65}(z, t) \right] \\ &\quad + W_{56}(z, t)N_{\text{Yb}} + R_{45}N_4(z, t)[N_{\text{Yb}} - N_6(z, t)] \\ &\quad - R_{60}N_6(z, t)[(1 - k)N_{\text{Nd}} - N_4(z, t)] \end{aligned} \quad (3)$$

$$\begin{aligned} \frac{\partial}{\partial t} \bar{N}_4(z, t) &= -\bar{N}_4(z, t) \left[\frac{1}{\tau_{\text{Nd}}} + W_{04}(z, t) + W_{40}(z, t) + W_{41}(z, t) \right] \\ &\quad + W_{04}(z, t)kN_{\text{Nd}} - \bar{R}_{40}\bar{N}_4(z, t)[kN_{\text{Nd}} - \bar{N}_4(z, t)]. \end{aligned} \quad (4)$$

Here, τ_{Nd} and τ_{Yb} are the spontaneous emission lifetimes of the $^4F_{3/2}$ and $^2F_{5/2}$ manifold states, respectively, and k is the fraction of Nd³⁺ ions in clusters. Note that the conservation relations $(1-k)N_{\text{Nd}} = N_0(z,t) + N_4(z,t)$, $kN_{\text{Nd}} = \bar{N}_0(z,t) + \bar{N}_4(z,t)$, and $N_{\text{Yb}} = N_5(z,t) + N_6(z,t)$ were used to eliminate $N_0(z,t)$, $\bar{N}_0(z,t)$, and $N_5(z,t)$ from (2)–(4). The forward and backward cross-relaxation coefficients are given by R_{45} and R_{60} , respectively. We employ the Forster–Dexter model [20] for dipole–dipole interactions in order to estimate the value of these coefficients in Nd³⁺-Yb³⁺ codoped glass (see, e.g., [5]). Assuming nearest neighbor interactions, R_{45} is estimated from [21]

$$R_{45} \simeq \left(\frac{4\pi}{3}\right)^2 \frac{1}{\tau_{\text{Nd}}} (N_{\text{Nd}} + N_{\text{Yb}}) r_0^6 \quad (5)$$

where r_0 is a critical interaction distance for Nd³⁺-Yb³⁺ energy transfer. This parameter is calculated from the spectral overlap of the Nd³⁺ emission and Yb³⁺ absorption cross sections [20]. In a similar manner, an expression for R_{60} can be derived. Other cross-relaxation coefficients in (2)–(4) include the homogeneous and intra-cluster rates R_{40} and \bar{R}_{40} , respectively. These rates cannot be derived from the Forster–Dexter model, due to the poor information on the $^4I_{9/2}$ - $^4I_{15/2}$ absorption cross section. We thus assume that the critical interaction distance r_0 for cross relaxation among homogeneous Nd³⁺ ions is of the same order of magnitude as the corresponding parameter for the Nd³⁺-Yb³⁺ cross relaxation.

The terms W_{04} and W_{40} stand for the Nd³⁺ pump absorption and stimulated emission rates, respectively, while the terms W_{56} and W_{65} are the Yb³⁺ absorption and stimulated emission rates, respectively. These terms depend on the pump power $P_p^\pm(z,t)$, and on the ASE power densities $P^\pm(z,t,\lambda)$, and are given by

$$\begin{aligned} W_{ij}(z,t) &= \frac{\Gamma_p}{hcA_{\text{core}}} \sum \sigma_{ij}(\lambda_p) [P_p^+(z,t) + P_p^-(z,t)] \lambda_p \\ &+ \frac{1}{hcA_{\text{core}}} \int \Gamma(\lambda) \sigma_{ij}(\lambda) [P^+(z,t,\lambda) + P^-(z,t,\lambda)] \lambda d\lambda. \end{aligned} \quad (6)$$

In (6), σ_{ij} is the wavelength-dependent cross section for radiative transition between levels i and j , h is the Planck constant, and c is the speed of light in a vacuum. The summation in (6) is over the multiplexed pump powers, while the limits of the integral are defined by the cross section of the $^4F_{3/2}$ - $^4I_{9/2}$ transitions of Nd³⁺ ions, and the cross section of the $^2F_{5/2}$ - $^2F_{7/2}$ transitions of Yb³⁺ ions. The stimulated transition rate W_{41} accounts for the ASE power emitted by the Nd³⁺ ions and is given by

$$\begin{aligned} W_{41}(z,t) &= \frac{1}{hcA_{\text{core}}} \int \Gamma(\lambda) \sigma_{41}(\lambda) [P^+(z,t,\lambda) + P^-(z,t,\lambda)] \lambda d\lambda \end{aligned} \quad (7)$$

where the limits of the integral in (7) are determined by the cross section of the $^4F_{3/2}$ - $^4I_{11/2}$ transitions of the Nd³⁺ ions. In these calculations, we assume that the ASE bandwidth is in the wavelength range from 840 to 1160 nm. We note that the Nd³⁺ transitions $^4F_{3/2}$ - $^4I_{13/2}$ at ~ 1300 nm can also contribute to the ASE power, but we found that this contribution is small for the range of parameters assumed in this work, and therefore, it was neglected. The rate of change of the ASE spectral power densities and the pump power along the fiber length are given below by (8) and (9). Here, $dP^\pm(z,t,\lambda)/dz \equiv \partial P^\pm/\partial z \pm (n/c)\partial P^\pm/\partial t$, and n is the refractive index of the core. The term $P_0(\lambda)$ in (8) denotes the contribution of the spontaneous emission to the power density of a single mode, and is given by $P_0(\lambda) = hc^2/\lambda^3$ [22]. Here, we assume that spontaneous emission events are equally likely for all propagating modes [23]. Thus, the fraction of spontaneous emission power that is coupled into all guiding modes is given by $\Gamma_{\text{se}}(\lambda) \equiv \sum_\eta g_\eta \Gamma_\eta(\lambda) I_\eta$ [15], [23]. The scattering loss $\alpha(\lambda)$ at wavelength λ also includes losses that are due to fiber coiling [24]. For simplicity, we assume that the scattering losses are constant. Nonlinear effects are not included in (8) and (9), shown at the bottom of the page, as recent experiments have shown that they are relatively weak for the range of pumping powers and fiber geometries that are assumed in this work [7]. In this work, we focus only on the steady-state solutions (i.e., $\partial/\partial t \equiv 0$) to the coupled rate-propagation equations (2)–(4), (8), and (9).

$$\begin{aligned} \pm \frac{dP^\pm(z,t,\lambda)}{dz} &= \left[\Gamma(\lambda) \left\{ [\sigma_{40}(\lambda) + \sigma_{41}(\lambda) + \sigma_{04}(\lambda)] [N_4(z,t) + \bar{N}_4(z,t)] - \sigma_{04}(\lambda) N_{\text{Nd}} \right. \right. \\ &\quad \left. \left. + [\sigma_{56}(\lambda) + \sigma_{65}(\lambda)] N_6(z,t) - \sigma_{56}(\lambda) N_{\text{Yb}} \right\} - \alpha(\lambda) \right] P^\pm(z,t,\lambda) \\ &+ \Gamma_{\text{se}}(\lambda) P_0(\lambda) \left[[\sigma_{41}(\lambda) + \sigma_{40}(\lambda)] [N_4(z,t) + \bar{N}_4(z,t)] + \sigma_{65}(\lambda) N_6(z,t) \right] \end{aligned} \quad (8)$$

$$\begin{aligned} \pm \frac{dP_p^\pm(z,t)}{dz} &= \left[\Gamma_p \left\{ [\sigma_{40}(\lambda_p) + \sigma_{04}(\lambda_p)] [N_4(z,t) + \bar{N}_4(z,t)] - \sigma_{04}(\lambda_p) N_{\text{Nd}} \right. \right. \\ &\quad \left. \left. + [\sigma_{56}(\lambda_p) + \sigma_{65}(\lambda_p)] N_6(z,t) - \sigma_{56}(\lambda_p) N_{\text{Yb}} \right\} - \alpha(\lambda_p) \right] P_p^\pm(z,t) \end{aligned} \quad (9)$$

We find that it is sufficient to assume reflectivity boundary conditions only for a single central wavelength λ_s of the DBR gratings [10], so that the power $P_s^\pm(z) = P^\pm(z, \lambda_s)\Delta\lambda_s$ at the lasing wavelength λ_s represents an average over the many resonances within a bandwidth $\Delta\lambda_s$. The integration of the rate-propagation equations is carried iteratively along the forward and backward propagation direction, until all the ASE power densities converge to a steady-state value [10]. On each integration step, the populations of homogeneous and clustered ions are found analytically by reducing (2) and (3) to a cubic equation and by reducing (4) to a quadratic equation for the unknowns $N_4(z)$ and $\bar{N}_4(z)$, respectively.

III. APPROXIMATE SOLUTION

We extend the approximate quasi-analytical solutions for single-doped Nd^{3+} - or Yb^{3+} -doped fiber lasers [10] to the Nd^{3+} - Yb^{3+} codoped system. We assume that Nd^{3+} ion-ion interactions can be neglected, so that all the Nd^{3+} ions are coupled to Yb^{3+} ions ($k \simeq 0$), and the cross-relaxation rates satisfy $R_{40} = \bar{R}_{40} \simeq 0$. Because of the smaller overlap of the Yb^{3+} emission band with the Nd^{3+} absorption band, the calculated backward energy transfer from Yb^{3+} to Nd^{3+} is considerably weaker than the forward energy transfer, and can safely be neglected. Therefore, we assume $R_{60} \simeq 0$. Furthermore, we assume strong pumping conditions, such that the oscillating laser power $P_s^\pm(z)$ is strong enough to allow neglecting the effect of the ASE on the gain. In this case, the gain of Nd^{3+} and Yb^{3+} ions is strongly saturated, and we have $N_4(z) \ll N_{\text{Nd}}$ and $N_6(z) \ll N_{\text{Yb}}$. Under these assumptions, the integration of (2), (3), (8), and (9) is considerably simplified, as described in the Appendix. In particular, we obtain a closed-form solution for the laser power, namely

$$P_s^\pm(z) = \frac{1}{2} \left[\sqrt{\Psi(z)^2 + B^2} \pm \Psi(z) \right] \quad (10)$$

where $\Psi(z)$ and the parameter B are defined in (A9) and (A10) in the Appendix, respectively. The function $\Psi(z)$ is derived from the numerical integration of (A12) (e.g., using the Runge-Kutta method) and is found by subsequently iterating the boundary condition (A13) (e.g., using bisection method), until convergence is achieved. This procedure is significantly faster and simpler to employ than the numerical solution of the exact (2), (3), (8), and (9).

IV. EXAMPLES

In what follows, we present a set of examples of high-power NYDFs, where we demonstrate the laser design optimization. The laser parameters that we consider are the pump power, pump configuration, fiber length, scattering loss, pump wavelengths, output mirror reflectivity, laser wavelength, and the Nd^{3+} and Yb^{3+} concentrations. We also compare the accuracy of the quasi-analytical solutions of the model to the exact numerical solution of the rate-propagation equations. It is assumed that the pump power is wavelength multiplexed, e.g., at $\lambda_p = 808$ nm, $\lambda_p = 940$ nm, and $\lambda_p = 976$ nm, so it pumps

TABLE I
PARAMETERS USED IN THE NUMERICAL CALCULATIONS

Parameter	Value	Notes
λ	1100 nm	
τ_{Nd}	0.4 msec	Ref. [10]
τ_{Yb}	1 msec	Ref. [10]
$\sigma_{41}(\lambda)$		Ref. [13]
$\sigma_{40}(\lambda)$		Ref. [25]
$\sigma_{04}(\lambda)$		Based on Ref. [26]
$\sigma_{56}(\lambda), \sigma_{65}(\lambda)$		Ref. [27]
R_{40}	$1.73 \times 10^{-24} \text{ m}^3\text{sec}^{-1}$	
\bar{R}_{40}	$1 \times 10^{-19} \text{ m}^3\text{sec}^{-1}$	Based on Ref. [28]
R_{45}	$5.5 \times 10^{-24} \text{ m}^3\text{sec}^{-1}$	
R_{60}	$1.92 \times 10^{-26} \text{ m}^3\text{sec}^{-1}$	
A_{core}	$4.714 \times 10^{-10} \text{ m}^2$	Ref. [7]
n	1.46	
NA	0.086	Ref. [7]
α	$5 \times 10^{-3} \text{ m}^{-1}$	
$\Gamma_\eta(\lambda)$		Ref. [15]
Γ_p	0.02	
L	35 m	Ref. [7]
$R_1(\lambda_s)$	0.98	
$R_2(\lambda_s)$	0.04	
N_{Nd}	$1.32 \times 10^{25} \text{ m}^{-3}$	Ref. [7]
N_{Yb}	$2.87 \times 10^{25} \text{ m}^{-3}$	Ref. [7]
k	0	

both the Nd^{3+} and the Yb^{3+} ions. Furthermore, we assume that the Bragg reflectors are centered at 1100 nm where both Nd^{3+} and Yb^{3+} ions have efficient optical transitions, and therefore the laser oscillates at this wavelength. The out-coupling mirror with the lower reflectivity is at $z = L$. Unless otherwise stated, the parameters used for the numerical calculations correspond closely to these of the experimental NYDFL described in [7], and are summarized in Table I.

In Fig. 2, we show the laser output power $P_{\text{out}}^+ = P_s^+(L)[1 - R_2(\lambda_s)]$, emitted from the output mirror at $z = L$, as a function of the total injected pump power $P_p(0)$. The lasing threshold is near $P_p = 890$ mW (see inset), and we note the linear increase of the output power without any sign of output power saturation at high pump power. This behavior is in contrast to other codoped laser systems, e.g., Er^{3+} - Yb^{3+} fibers [11], where the so-called energy-transfer ‘‘bottleneck’’ limits the efficiency of the system. The slope efficiency ($\eta_D \equiv \Delta P_{\text{out}}^+ / \Delta P_p$) of the laser is about 0.71, which is in good agreement with the 0.72 efficiency reported in recent experiments [7]. Similar results are obtained with respect to the absorbed pump power, which indicate a very efficient pump-power absorption in the fiber. The calculated threshold of the quasi-analytical solution is about 920 mW, which is in good agreement with the exact numerical value. We note that the approximate quasi-analytical solution becomes less accurate as the pump power is increased, and that the slope obtained from the approximate solution is lower than that of the exact solution. This deviation is a result of the contribution of the $\lambda_p = 976$ nm wavelength to $P_p^+(z)$, which is not exactly exponential, as predicted by (A11). In particular,

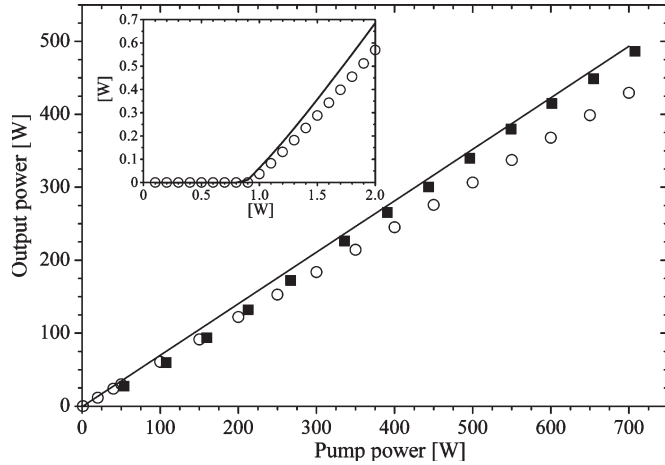


Fig. 2. Output power as a function of the input pump power $P_p(0)$. The pump power is divided among three different pump wavelengths at $\lambda_p = 976$ nm, $\lambda_p = 940$ nm, and $\lambda_p = 808$ nm, with power of $P_p(0)/2$, $P_p(0)/4$, and $P_p(0)/4$, respectively. The solid lines represent the exact solution of (2), (3), (8), and (9), whereas the circles represent the approximate quasi-analytical solution obtained from (10) and (A12). The rectangles represent experimental results obtained from [7]. The inset shows the output power near the lasing threshold.

under strong pumping conditions, the population $N_6(z)$ builds up significantly near the injected pump end at $z = 0$, and the condition $N_6(z) \ll N_{Yb}$ leading to the approximate (A11) is not satisfied.

In Fig. 3, we show the laser slope efficiency (η_D) and the laser threshold power as a function of the laser length (L). We note that there is a good agreement between the quasi-analytical solution and the exact solution over the entire range of fiber lengths and scattering loss (α). The dependence of the slope efficiency on the fiber length is in qualitative agreement with results obtained for the conversion efficiency ($\eta_c \equiv P_{out}^+/P_p$) of typical strongly pumped fiber lasers [10]. That is, the slope efficiency increases with the fiber length until it saturates. This increase strongly depends on the scattering loss, and is achieved in shorter fiber lengths for higher scattering loss, but with lower efficiency. The slope efficiency also depends on the pumping configuration and higher slope efficiencies can be obtained by pumping at $z = L$. For example, for scattering loss $\alpha_s = 5 \times 10^{-3} \text{ m}^{-1}$ the fiber lengths where the slope efficiency is maximized are approximately 24 m for pumping at $z = 0$ and 33 m for pumping at $z = L$. If the scattering loss is larger, i.e., $\alpha_s = 5 \times 10^{-2} \text{ m}^{-1}$, the corresponding figures are 9 m for pumping at $z = 0$ and 13 m for pumping at $z = L$. On the other hand, the laser threshold shows only weak dependence on the pumping configuration, as expected, and it is more strongly affected by the scattering losses.

Next, we consider a few examples of a laser design optimization, in which we select the optimal laser length for maximizing the laser output power and hence the laser conversion efficiency. Fig. 4 shows the effect of multiplexing two pump sources with different wavelengths on the laser efficiency. The figure depicts contour lines of (a) the optimal laser length and (b) the corresponding output power, as a function of a pump wavelength in the Nd³⁺ absorption band (in the range 700–850 nm) and a pump wavelength in the Yb³⁺ absorption band (in the range 850–1050 nm). We note the existence of

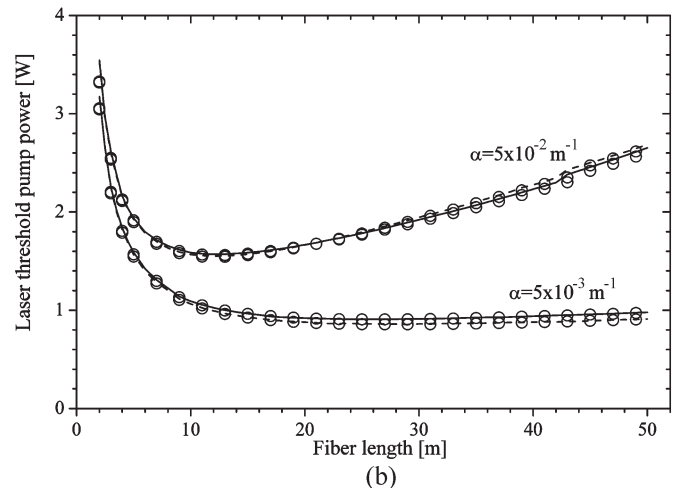
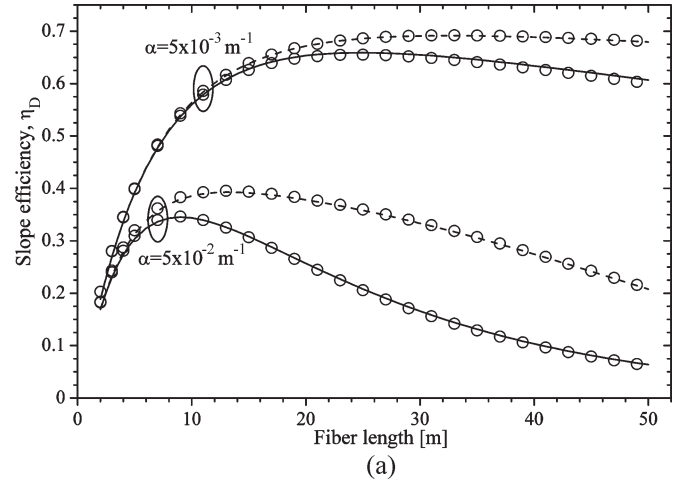


Fig. 3. (a) Laser slope efficiency and (b) laser threshold pump power, as a function of the fiber length (L), for two values of the scattering loss (α), and for an input pump power of $P_p = 500$ W divided equally among $\lambda_p = 940$ nm and $\lambda_p = 808$ nm. The solid and dashed lines represent the exact solution of (2), (3), (8), and (9), for pumping at $z = 0$ or at $z = L$, respectively. The circles represent the approximate quasi-analytical solution obtained from (10) and (A12).

two Nd³⁺ pump wavelengths around $\lambda_p = 745$ nm and $\lambda_p = 808$ nm, where the optimal laser length is not sensitive to the choice of the Yb³⁺ pump wavelength for a wide range of wavelengths between $\lambda_p = 880$ nm to $\lambda_p = 940$ nm. The highest efficiency is achieved at pump wavelengths where both the Nd³⁺ and Yb³⁺ pump absorptions are maximized, e.g., on pumping the Yb³⁺ at $\lambda_p = 976$ nm and Nd³⁺ at $\lambda_p = 808$ nm. We note that the efficiency decreases on changing the Yb³⁺ pump wavelength from $\lambda_p = 976$ nm to $\lambda_p = 940$ nm by less than 10%. Thus, the Yb³⁺ pump wavelength selection is more limited by the optimal laser length, which should be kept short enough to reduce the effect of fiber nonlinearities.

In Fig. 5, we show a contour plot of (a) the optimal laser length and (b) the corresponding output power, as a function of the laser wavelength and the output mirror reflectivity at $z = L$. It is found that for sufficiently high output mirror reflectivities ($R_2 > 5 \times 10^{-3}$), the optimal laser length is not sensitive to the choice of the laser wavelength λ_s , as long as $\lambda_s \gtrsim 1045$ nm. For example, the optimal laser length in the spectral range $1050 \text{ nm} \lesssim \lambda_s \lesssim 1130 \text{ nm}$ is about 24 m, for

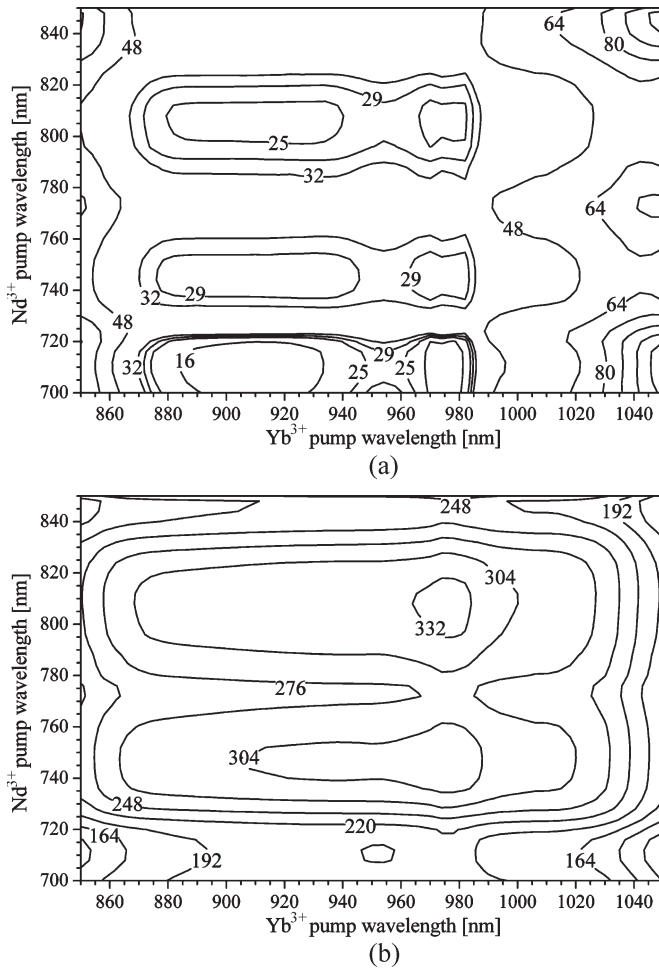


Fig. 4. Calculated contour plots of the (a) optimal laser length (in meters) and (b) corresponding output power (in watts), as a function of Nd³⁺ and Yb³⁺ pump wavelengths, for an input pump power of $P_p(0) = 500$ W divided equally.

an output mirror reflectivity of $R_2 \approx 8 \times 10^{-2}$. This spectral width of constant optimal length becomes broader as the output mirror reflectivity becomes higher. We conclude that an optimum use of the same laser cavity can be realized for a range of laser wavelengths, which can be important for tunable laser applications. There exists an optimum laser wavelength for obtaining the highest efficiency, i.e., $\lambda_s \approx 1050$ nm; however, it is at an extremely small optimum output mirror reflectivity ($R_2 \approx 10^{-5}$). For shorter wavelengths ($\lambda_s < 1050$ nm), the output power is limited by a strongly competing ASE due to the transitions at $\lambda \approx 1060$ nm, and the output mirror reflectivity should be increased in order to suppress this ASE and reach threshold. For longer wavelengths ($\lambda_s > 1050$ nm), the decrease in the laser output power is due to the smaller Nd³⁺ and Yb³⁺ emission cross sections, and the long wavelength limit of the laser tuning is eventually fixed by the laser cutoff conditions. In relation to these results, we note that the laser output power can be tuned across a somewhat larger spectral bandwidth compared with pure Nd³⁺- or Yb³⁺-doped fiber lasers [13]. Furthermore, some control over the gain spectrum can be achieved via selection of the relative dopant concentrations, which might offer more tuning flexibility compared with

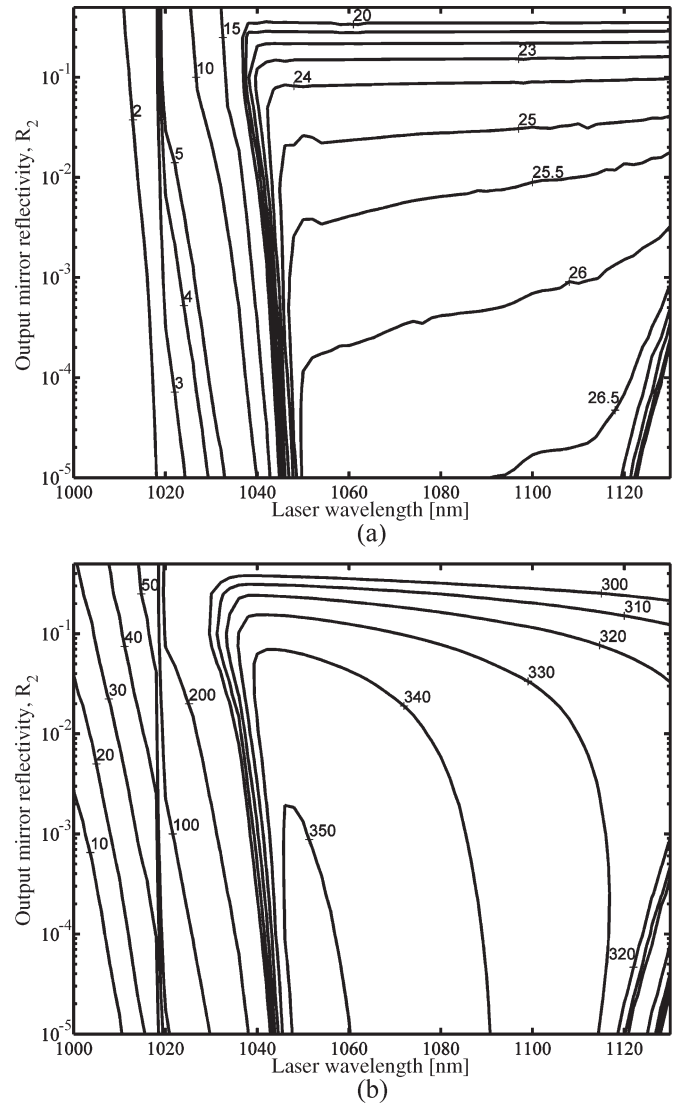


Fig. 5. Calculated contour plots of the (a) optimal laser length (in meters) and (b) corresponding output power (in watts), as a function of the laser wavelength (λ_s) and the output mirror reflectivity at $z = L(R_2)$, for an input pump power of $P_p(0) = 500$ W divided equally among $\lambda_p = 940$ nm and $\lambda_p = 808$ nm.

pure lasers. It is also worth to mention that the laser output power tuning depends on the choice of the glass host, which modifies the cross sections of both Nd³⁺ and Yb³⁺ ions.

Other important design parameters that we consider are the Nd³⁺ and Yb³⁺ concentrations. In Fig. 6, we plot the contour lines of the optimal laser length and the corresponding output power versus the Yb³⁺ concentration and the Nd³⁺-Yb³⁺ ratio. The optimal laser length is found to be strongly dependent on the Yb³⁺ concentration and much less on the Nd³⁺ concentration, in particular in the limit of high Nd³⁺-Yb³⁺ ratios. We note that the optimal length generally decreases with increasing Yb³⁺ concentration. The highest efficiency that can be obtained from the laser on variation of the Yb³⁺ and Nd³⁺ concentrations is approximately 0.77. Further increase is ultimately limited by concentration quenching effects, e.g., the formation of Yb³⁺ ion clusters that inhibit the Nd³⁺-Yb³⁺ energy transfer and can self-absorb the emitted light. On increasing the Nd³⁺-Yb³⁺ ratio, the efficiency first increases

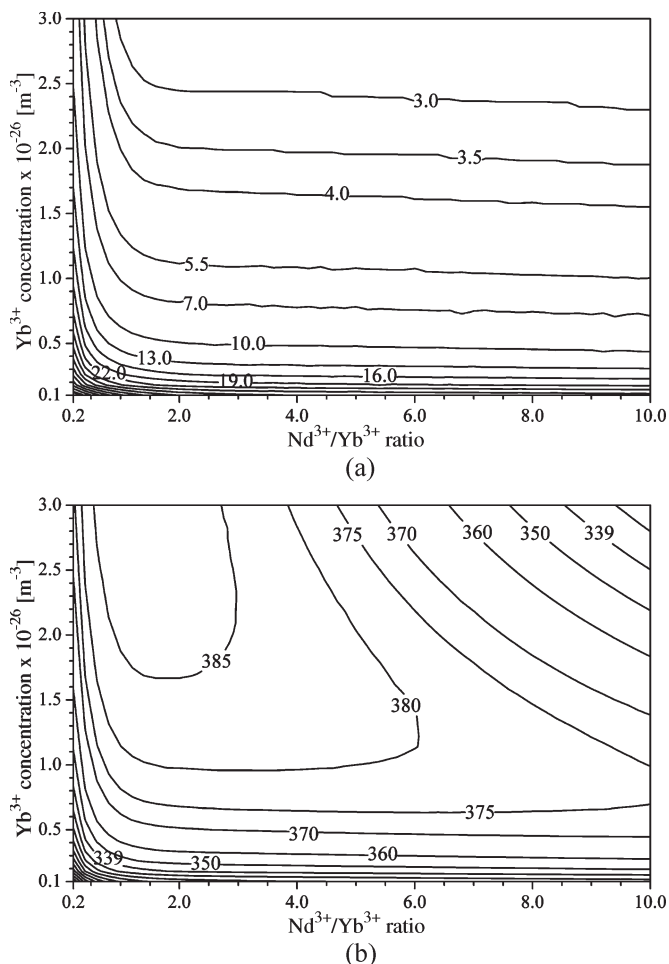


Fig. 6. Calculated contour plots of the (a) optimal laser length (in meters) and (b) corresponding output power (in watts), as a function of the Yb^{3+} concentration (N_{Yb}) and the Nd^{3+} - Yb^{3+} ratio, for an input pump power of $P_p(0) = 500$ W divided equally among $\lambda_p = 940$ nm and $\lambda_p = 808$ nm.

due to the improved pump absorption, then reaches an optimum value and decreases. This saturation effect is a consequence of the cross-relaxation losses of Nd^{3+} ions, which are more significant in higher Nd^{3+} concentrations where the average distance between two Nd^{3+} ions is smaller.

The importance of Nd^{3+} ion-ion interactions for the laser efficiency is further illustrated in Fig. 7. Here, we present the output power of an optimal length NYDFL versus the Nd^{3+} concentration, with the fraction of clustered Nd^{3+} ions (k) as a parameter. The corresponding dependence of the optimal laser length is similar to that of Fig. 6, i.e., it decreases with the Nd^{3+} concentration, more strongly in the limit of small Nd^{3+} concentrations. The highest efficiency that can be obtained by the variation of the Nd^{3+} concentration depends on the amount of Nd^{3+} clusters in the system. In particular, as the fraction of Nd^{3+} ions in the clusters is increased, the efficiency of the NYDFL decreases, and the optimal Nd^{3+} concentration becomes smaller. We note the difference between the effect of Nd^{3+} clusters in this system, to the effect of Er^{3+} clusters in Er^{3+} -doped systems. While in the four-level system of Nd^{3+} , the clusters lower the population density of the $^4F_{3/2}$ manifold due to an increase in the cross-relaxation rate, as well as reduce the number of Nd^{3+} ions that interact with Yb^{3+} , the three-

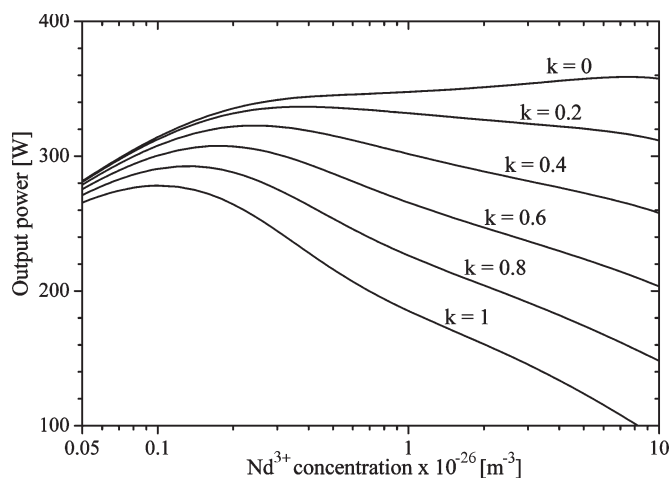


Fig. 7. Calculated output power at the optimal laser length as a function of the Nd^{3+} concentration (N_{Nd}), for different fraction of Nd^{3+} in clusters (k). The input pump power $P_p(0) = 500$ W is divided equally among $\lambda_p = 940$ nm and $\lambda_p = 808$ nm.

level Er^{3+} clusters absorb the signal that is emitted and amplified by the homogeneous ions. Therefore, the decrease of the NYDFL efficiency due to an increase in the number of clustered ions is less significant than in three-level systems (e.g., see [17]). For example, the maximum efficiency of a system with full clustering ($k = 1$) is 0.56, for a Nd^{3+} concentration of $N_{\text{Nd}} \simeq 1 \times 10^{25} \text{ m}^{-3}$, whereas the corresponding figures for a system with no clustering ($k = 0$) are 0.73 and $N_{\text{Nd}} \simeq 8.5 \times 10^{26} \text{ m}^{-3}$, respectively.

V. CONCLUSION

We presented a theoretical analysis of high-power NYDFLs, based on a detailed rate-propagation equation model that takes into account the energy transfer between Nd^{3+} and Yb^{3+} , cross relaxation in the Nd^{3+} ion system, and the propagation of higher order modes. We considered examples of cladding-pumped NYDFLs operating at spectral bandwidth in the vicinity of 1100 nm, where both the Nd^{3+} and Yb^{3+} have efficient optical transitions. Our results demonstrate the high slope efficiency of NYDFLs, about 0.71, in agreement with recent experimental results [7]. It has been shown, that pumping at $z = L$ leads to higher slope efficiencies, particularly in the limit of longer fibers. On the other hand, the pumping configuration has been shown to have only a small effect on the laser threshold. The optimal fiber length for achieving the maximum output power can be found by tuning the Nd^{3+} and Yb^{3+} pump wavelengths and is not sensitive to the pump wavelength selection within a large bandwidth of the Yb^{3+} absorption band. Pumping at $z = 0$ with pump wavelengths of $\lambda_p = 940$ nm and $\lambda_p = 808$ nm, the optimal fiber length is ~ 24 m, the slope efficiency is ~ 0.66 , and the laser threshold is ~ 0.91 W. In practice, however, the choice of the fiber length and hence the achievable output power are limited due to fiber nonlinearities. On increasing the Yb^{3+} concentration, the laser becomes more efficient, whereas the optimal Nd^{3+} concentration is limited by concentration quenching. In particular, Nd^{3+} clustering effects can reduce the maximum output power of the NYDFL.

Assuming a typical value of 18% of the Nd^{3+} ions in clusters [28], we find that the optimum Nd^{3+} concentration is $\sim 4 \times 10^{25} \text{ m}^{-3}$. We have shown that the laser wavelength can be tuned in wide range, e.g., from about 1050 to 1120 nm (and beyond), with only small variation in the optimal laser length, provided the mirror reflectivity is high enough.

An approximate quasi-analytical solution to the model equations was derived and compared with the exact numerical calculations. It was shown that the approximate solutions are in good agreement with the exact solutions for a range of fiber lengths and pumping configurations. The approximate solutions become less accurate when pumping at $\lambda_p = 976 \text{ nm}$, particularly in the limit of high pump power.

APPENDIX QUASI-ANALYTICAL SOLUTION OF (2), (3), (8), AND (9)

The mathematical description of the optical power spectrum propagating in the laser cavity can be significantly simplified by assuming that the oscillating laser power is strong enough to neglect the influence of the ASE on the population inversion of Nd^{3+} and Yb^{3+} ions. That is, we assume $P^\pm(z, \lambda) = P_s^\pm(z)\delta(\lambda - \lambda_s)$. We also ignore the effect of cross relaxation among Nd^{3+} ions, i.e., we assume $k \simeq 0$ and $R_{40} = \bar{R}_{40} \simeq 0$. In this case, (8) reduces to

$$\pm \frac{1}{P_s^\pm(z)} \frac{dP_s^\pm(z)}{dz} = g_s(z) - \alpha(\lambda_s) \quad (\text{A1})$$

where $g_s(z)$ is the differential signal gain per unit length at $\lambda = \lambda_s$. We consider only lasing transitions in the Nd^{3+} ions around the 1060-nm emission band. Therefore, $g_s(z) \equiv \Gamma_s(\sigma_{41}(\lambda_s)N_4(z) + [\sigma_{65}(\lambda_s) + \sigma_{56}(\lambda_s)]N_6(z) - \sigma_{56}(\lambda_s)N_{\text{Yb}})$, where $\Gamma_s \equiv \Gamma(\lambda_s)$. We further limit ourselves to high laser power circulating the cavity, such that the constituent ion gain is saturated, i.e., we assume $N_4(z) \ll N_{\text{Nd}}$ and $N_6(z) \ll N_{\text{Yb}}$. Employing these assumptions to (2) and (3), one obtains for the differential signal gain

$$g_s(z) \simeq \frac{g_0^{\text{Nd}}(z)}{f_{\text{Nd}}(z) + \frac{P_s^+(z) + P_s^-(z)}{P_{\text{sat}}^{\text{Nd}}}} + \frac{g_0^{\text{Yb}}(z)}{f_{\text{Yb}}(z) + \frac{P_s^+(z) + P_s^-(z)}{P_{\text{sat}}^{\text{Yb}}}} \quad (\text{A2})$$

where $f_{\text{Nd}}(z)$, $g_0^{\text{Nd}}(z)$, and $P_{\text{sat}}^{\text{Nd}}$ are parameters related to the gain due to the Nd^{3+} ions and are defined by

$$f_{\text{Nd}}(z) \equiv 1 + \tau_{\text{Nd}}R_{45} [N_{\text{Yb}} - N_6(z)] + \frac{\Gamma_p \tau_{\text{Nd}}}{hcA_{\text{core}}} \sum \sigma_{40}(\lambda_p)\lambda_p [P_p^+(z) + P_p^-(z)] \quad (\text{A3})$$

$$g_0^{\text{Nd}}(z) \equiv \frac{N_{\text{Nd}}\Gamma_p}{\lambda_s P_{\text{sat}}^{\text{Nd}}} \sum \sigma_{04}(\lambda_p)\lambda_p [P_p^+(z) + P_p^-(z)] \quad (\text{A4})$$

$$P_{\text{sat}}^{\text{Nd}} \equiv \frac{hcA_{\text{core}}}{\Gamma_s \sigma_{41}(\lambda_s)\lambda_s \tau_{\text{Nd}}} \quad (\text{A5})$$

where the summation is over the multiplexed pump powers. The parameters $f_{\text{Yb}}(z)$, $g_0^{\text{Yb}}(z)$, and $P_{\text{sat}}^{\text{Yb}}$ are related to the gain due to the Yb^{3+} ions and are defined by

$$f_{\text{Yb}}(z) \equiv 1 + \frac{\Gamma_p \tau_{\text{Yb}}}{hcA_{\text{core}}} \sum \sigma_{65}(\lambda_p)\lambda_p [P_p^+(z) + P_p^-(z)] \quad (\text{A6})$$

$$g_0^{\text{Yb}}(z) \equiv \frac{N_{\text{Yb}}\Gamma_p\Gamma_s [\sigma_{65}(\lambda_s) + \sigma_{56}(\lambda_s)] \tau_{\text{Yb}}}{hcA_{\text{core}}} \times \sum \sigma_{56}(\lambda_p)\lambda_p [P_p^+(z) + P_p^-(z)] + \Gamma_s [\sigma_{65}(\lambda_s) + \sigma_{56}(\lambda_s)] N_{\text{Yb}}R_{45}\tau_{\text{Yb}}N_4(z) - \sigma_{56}(\lambda_s)N_{\text{Yb}}\Gamma_s f_{\text{Yb}}(z) + \Gamma_s \frac{[\sigma_{56}(\lambda_s)]^2}{\sigma_{65}(\lambda_s)} N_{\text{Yb}} \frac{\sqrt{\Psi^2(z) + B^2}}{P_{\text{sat}}^{\text{Yb}}} \quad (\text{A7})$$

$$P_{\text{sat}}^{\text{Yb}} \equiv \frac{hcA_{\text{core}}}{\Gamma_s \sigma_{65}(\lambda_s)\lambda_s \tau_{\text{Yb}}} \quad (\text{A8})$$

Note that for improved computational stability, particularly at lasing wavelengths where $\sigma_{56}(\lambda_s) \ll \sigma_{65}(\lambda_s)$, the last term in the RHS of (A7) can be omitted. The dimensionless function $\Psi(z)$ and the constant parameter B are defined as follows:

$$\Psi(z) \equiv P_s^+(z) - P_s^-(z) \quad (\text{A9})$$

$$B \equiv 2\sqrt{P_s^+(z)P_s^-(z)}. \quad (\text{A10})$$

From (A9) and (A10), we obtain (10) in the text for the propagating signal power $P_s^\pm(z)$ in terms of $\Psi(z)$ and B . Also, by further assuming that $\sigma_{65}(\lambda_p) \ll \sigma_{56}(\lambda_p)$ and $\sigma_{40}(\lambda_p) \ll \sigma_{04}(\lambda_p)$, (9) is analytically integrable to yield the forward and backward propagating pump power at wavelength $\lambda = \lambda_p$

$$P_p^+(z) = P_p^+(0) \exp \left\{ - \left[\Gamma_p (\sigma_{56}(\lambda_p)N_{\text{Yb}} + \sigma_{04}(\lambda_p)N_{\text{Nd}}) + \alpha(\lambda_p) \right] z \right\}$$

$$P_p^-(z) = P_p^-(L) \exp \left\{ - \left[\Gamma_p (\sigma_{56}(\lambda_p)N_{\text{Yb}} + \sigma_{04}(\lambda_p)N_{\text{Nd}}) + \alpha(\lambda_p) \right] (L - z) \right\}. \quad (\text{A11})$$

Substituting (A2) in (A1) for $P_s^\pm(z)$ and employing (A9) and (A10), we obtain the following differential equation for $\Psi(z)$:

$$\frac{d\Psi(z)}{dz} = \left[\frac{g_0^{\text{Nd}}(z)}{f_{\text{Nd}}(z) + \frac{\sqrt{\Psi^2(z) + B^2}}{P_{\text{sat}}^{\text{Nd}}}} + \frac{g_0^{\text{Yb}}(z)}{f_{\text{Yb}}(z) + \frac{\sqrt{\Psi^2(z) + B^2}}{P_{\text{sat}}^{\text{Yb}}}} - \alpha(\lambda_s) \right] \sqrt{\Psi^2(z) + B^2} \quad (\text{A12})$$

where the boundary conditions for (A12) are given by [10]

$$\Psi(L) = -\frac{[1 - R_2(\lambda_s)]\sqrt{R_1(\lambda_s)}}{[1 - R_1(\lambda_s)]\sqrt{R_2(\lambda_s)}}\Psi(0). \quad (\text{A13})$$

The numerical integration of the approximate (A12) is referred to as the quasi-analytical solution. To this end, the parameter B can be expressed in terms of the boundary conditions $\Psi(0)$ and $\Psi(L)$ [10]. Furthermore, it is straightforward to obtain closed-form analytical solutions for the population inversions of the Nd³⁺ and Yb³⁺ ions, namely, $N_4(z)$ and $N_6(z)$, using (2) and (3). The quasi-analytical solution is significantly faster than the iterative numerical solution of the exact (2), (3), (8), and (9).

ACKNOWLEDGMENT

The authors would like to thank M. Puterkovsky for the discussions.

REFERENCES

- [1] V. Dominic, S. McCormack, R. Waarts, S. Sanders, S. Bicknese, R. Dohle, E. Wolak, P. S. Yeh, and E. Zucker, "110 W fiber laser," *Electron. Lett.*, vol. 35, no. 14, pp. 1158–1160, Jul. 1999.
- [2] C. H. Liu, B. Ehlers, F. Doerfel, S. Heinemann, A. Carter, K. Tankala, J. Farroni, and A. Galvanauskas, "810 W continuous-wave and single-transverse-mode fibre laser using 20 μm core Yb-doped double-clad fibre," *Electron. Lett.*, vol. 40, no. 23, pp. 1471–1472, Nov. 2004.
- [3] Y. Jeong, J. K. Sahu, D. N. Payne, and J. Nilsson, "Ytterbium-doped large-core fiber laser with 1.36 kW continuous-wave output power," *Opt. Express*, vol. 12, no. 25, pp. 6088–6092, Dec. 2004.
- [4] E. Snitzer, "Laser emission at 1.06 μ from Nd³⁺-Yb³⁺ glass," *IEEE J. Quantum Electron.*, vol. QE-2, no. 9, pp. 562–566, Sep. 1966.
- [5] D. F. deSousa, F. Batalioto, M. J. V. Bell, S. L. Oliveira, and L. A. O. Nunes, "Spectroscopy of Nd³⁺ and Yb³⁺ codoped fluorindogallate glasses," *J. Appl. Phys.*, vol. 90, no. 7, pp. 3308–3313, Oct. 2001.
- [6] J. Limpert, A. Liem, S. Hofer, H. Zellmer, and A. Tunnermann, "150 W Nd/Yb codoped fiber laser at 1.1 μm ," in *Proc. Conf. Lasers and Electro-Optics*, Long Beach, CA, 2001, pp. 590–591. Paper CThX1.
- [7] J. Limpert, A. Liem, H. Zellmer, and A. Tunnermann, "500 W continuous-wave fibre laser with excellent beam quality," *Electron. Lett.*, vol. 39, no. 8, pp. 645–647, Apr. 2003.
- [8] N. G. R. Broderick, H. L. Offerhaus, D. J. Richardson, R. A. Sammut, J. Caplen, and L. Dong, "Large mode area fibers for high power applications," *Opt. Fiber Technol.*, vol. 5, no. 2, pp. 185–196, Apr. 1999.
- [9] J. P. Kopolow, D. A. V. Kliner, and L. Goldberg, "Single-mode operation of a coiled multimode fiber amplifier," *Opt. Lett.*, vol. 25, no. 7, pp. 442–444, Apr. 2000.
- [10] I. Kelson and A. A. Hardy, "Strongly pumped fiber lasers," *IEEE J. Quantum Electron.*, vol. 34, no. 9, pp. 1570–1577, Sep. 1998.
- [11] E. Yahiel and A. Hardy, "Modeling high-power Er³⁺-Yb³⁺ codoped fiber lasers," *J. Lightw. Technol.*, vol. 21, no. 9, pp. 2044–2052, Sep. 2003.
- [12] H. Zellmer, U. Willamowski, A. Tunnermann, H. Welling, S. Unger, V. Reichel, H. R. Muller, J. Kirchhof, and P. Albers, "High-power cw neodymium-doped fiber laser operating at 9.2 W with high beam quality," *Opt. Lett.*, vol. 20, no. 6, pp. 578–580, Mar. 1995.
- [13] J. Nilsson, W. A. Clarkson, R. Selvas, J. K. Sahu, P. W. Turner, S. U. Alam, and A. B. Grudinin, "High-power wavelength-tunable cladding-pumped rare-earth-doped silica fiber lasers," *Opt. Fiber Technol.*, vol. 10, no. 1, pp. 5–30, Jan. 2004.
- [14] A. W. Snyder and C. Pask, "Incoherent illumination of an optical fiber," *J. Opt. Soc. Amer.*, vol. 63, no. 7, pp. 806–812, Jul. 1973.
- [15] A. W. Snyder and J. D. Love, *Optical Waveguide Theory*. New York: Chapman & Hall, 1983.
- [16] D. Gloge, "Weakly guiding fibers," *Appl. Opt.*, vol. 10, no. 10, pp. 2252–2258, Oct. 1971.
- [17] E. Yahiel and A. Hardy, "Efficiency optimization of high-power, Er³⁺-Yb³⁺-codoped fiber amplifiers for wavelength-division-multiplexing applications," *J. Opt. Soc. Amer. B, Opt. Phys.*, vol. 20, no. 6, pp. 1189–1197, Jun. 2003.
- [18] B. J. Ainslie, S. P. Craig, S. T. Davey, D. J. Barber, J. R. Taylor, and A. S. L. Gomes, "Optical and structural investigations of Nd³⁺ in silica-based fibres," *J. Mater. Sci. Lett.*, vol. 6, no. 11, pp. 1361–1363, Nov. 1987.
- [19] K. Arai, H. Hamikawa, K. Kumata, T. Honda, Y. Ishli, and T. Handa, "Aluminum or phosphorus co-doping effects on the fluorescence and structural properties of neodymium-doped silica glass," *J. Appl. Phys.*, vol. 59, no. 10, pp. 3430–3436, May 1986.
- [20] D. L. Dexter, "A theory of sensitized luminescence in solids," *J. Chem. Phys.*, vol. 21, no. 5, pp. 836–850, May 1953.
- [21] C. Y. Chen, R. R. Petrin, D. C. Yeh, A. W. Sibley, and J. L. Adam, "Concentration-dependent energy-transfer processes in Er³⁺ and Tm³⁺-doped heavy-metal fluoride glass," *Opt. Lett.*, vol. 14, no. 9, pp. 432–434, May 1989.
- [22] C. H. Henry, "Theory of spontaneous emission noise in open resonators and its application to lasers and optical amplifiers," *J. Lightw. Technol.*, vol. LT-4, no. 3, pp. 288–297, Mar. 1986.
- [23] E. Desurvire, *Erbium-Doped Fiber Amplifiers: Principles and Applications*. New York: Wiley, 2002.
- [24] M. Ohashi and K. Shiraki, "Bending loss effect on signal gain in an Er³⁺-doped fiber amplifier," *IEEE Photon. Technol. Lett.*, vol. 4, no. 2, pp. 192–194, Feb. 1992.
- [25] W. J. Miniscalco, "Optical and electronic properties of rare earth ions in glasses," in *Rare-Earth-Doped Fiber Lasers and Amplifiers*, 2nd ed. M. J. F. Digonnet, Ed. New York: Marcel Dekker, 2001, pp. 17–112.
- [26] L. Reekie, I. M. Jauncey, S. B. Poole, and D. N. Payne, "Diode-laser-pumped Nd³⁺-doped fibre laser operating at 938 nm," *Electron. Lett.*, vol. 23, no. 17, pp. 884–885, Aug. 1987.
- [27] R. Paschotta, J. Nilsson, A. C. Tropper, and D. C. Hanna, "Ytterbium-doped fiber amplifiers," *IEEE J. Quantum Electron.*, vol. 33, no. 7, pp. 1049–1056, Jul. 1997.
- [28] M. K. Davis, M. J. F. Digonnet, and R. H. Pantell, "Characterization of clusters in rare earth-doped fibers by transmission measurements," *J. Lightw. Technol.*, vol. 13, no. 2, pp. 120–126, Feb. 1995.

Eldad Yahiel, photograph and biography not available at the time of publication.

Ortwin Hess, photograph and biography not available at the time of publication.

Amos A. Hardy (SM'84–F'97), photograph and biography not available at the time of publication.